Chemical Engineering Science 65 (2010) 726–738

Contents lists available at ScienceDirect

Chemical Engineering Science

journal homepage: www.elsevier.com/locate/ces

Computational study of forced convective heat transfer in structured packed beds with spherical or ellipsoidal particles

Jian Yang [a], Qiuwang Wang [a,*], Min Zeng [a], Akira Nakayama [b]

[a] State Key Laboratory of Multiphase Flow in Power Engineering, Xi'an Jiaotong University, Xi'an, Shaanxi 710049, PR China
[b] Department of Mechanical Engineering, Shizuoka University, 3-5-1 Johoku, Hamamatsu 432, Japan

ARTICLE INFO

Article history:
Received 2 December 2008
Received in revised form
30 July 2009
Accepted 11 September 2009
Available online 25 September 2009

Keywords:
Computational fluid dynamics
Packed bed
Ellipsoidal particle
Laminar flow
Turbulence
Heat transfer

ABSTRACT

Randomly packed bed reactors are widely used in chemical process industries, because of their low cost and ease of use compared to other packing methods. However, the pressure drops in such packed beds are usually much higher than those in other packed beds, and the overall heat transfer performances may be greatly lowered. In order to reduce the pressure drops and improve the overall heat transfer performances of packed beds, structured packed beds are considered to be promising choices. In this paper, the flow and heat transfer inside small pores of some novel structured packed beds are numerically studied, where the packed beds with ellipsoidal or non-uniform spherical particles are investigated for the first time and some new transport phenomena are obtained. Three-dimensional Navier–Stokes equations and RNG k–ε turbulence model with scalable wall function are adopted for present computations. The effects of packing form and particle shape are studied in detail and the flow and heat transfer performances in uniform and non-uniform packed beds are also compared with each other. Firstly, it is found that, with proper selection of packing form and particle shape, the pressure drops in structured packed beds can be greatly reduced and the overall heat transfer performances will be improved. The traditional correlations of flow and heat transfer extracted from randomly packings are found to overpredict the pressure drops and Nusselt number for all these structured packings, and new correlations of flow and heat transfer are obtained. Secondly, it is also revealed that, both the effects of packing form and particle shape are significant on the flow and heat transfer in structured packed beds. With the same particle shape (sphere), the overall heat transfer efficiency of simple cubic (SC) packing is the highest. With the same packing form, such as face center cubic (FCC) packing, the overall heat transfer performance of long ellipsoidal particle model is the best. Furthermore, with the same particle shape and packing form, such as body center cubic (BCC) packing with spheres, the overall heat transfer performance of uniform packing model is higher than that of non-uniform packing model. The models and results presented in this paper would be useful for the optimum design of packed bed reactors.

1. Introduction

Packed beds, due to their high surface area-to-volume ratio, are widely used in chemical process industries, such as catalytic reactors, chromatographic reactors, ion exchange columns and absorption towers (Caulkin et al., 2007).

In industrial applications, randomly packed beds are prevailing for decades because of their low cost and ease of use compared to other packing methods. Nijemeisland and Dixon (2004) studied the flow and wall heat transfer performance in a randomly packed bed of spheres. CFD method was used for obtaining the detailed velocity and temperature fields for gas flowing through a periodic wall segment test cell. They found that, local heat transfer rates did not correlate statistically with the local flow field but related to larger-scale flow structures in the bed. Single phase reacting flows in a randomly packed bed reactor were investigated by Freund et al. (2003) with LBM method. They found that, not only the local behavior but also the integral quantities, such as the pressure drop, depended remarkably on the local structural properties of the packings. Guardo et al. (2005) presented a comparison between the performance in flow and heat transfer estimation of five different RANS turbulence models in a randomly packed bed composed of 44 homogeneous stacked spheres. They found that, the Spalart–Allmaras turbulence model was better than the two-equation RANS models for pressure drop and heat transfer parameter estimation. The computational results of pressure drop and heat transfer coefficient agreed well

Abbreviations: SC, simple cubic; FCC, face center cubic; BCC, body center cubic; CFD, computational fluid dynamics

* Corresponding author. Tel./fax: +86 29 82663502.
E-mail address: wangqw@mail.xjtu.edu.cn (Q. W. Wang).

0009-2509/$ - see front matter © 2009 Elsevier Ltd. All rights reserved.
doi:10.1016/j.ces.2009.09.026

with those calculated by traditional empirical correlations (Ergun, 1952; Wakao and Kaguei, 1982). Guardo et al. (2006, 2007) performed similar studies for randomly packed beds later. CFD method was proved to be a reliable tool when modeling convective heat transfer phenomena in packed beds.

However, the flow and heat transfer performances of randomly packed beds may not be optimal, the pressure drops in such packed beds are usually much higher than those in other packed beds (Calis et al., 2001), and the overall heat transfer performances may be greatly lowered. In order to reduce the pressure drops and improve the overall heat transfer performances of packed beds, structured packed beds may be used instead of traditional randomly packed beds. Susskind and Becker (1967) measured the pressure drop of water when it flowed through a bed of stainless steel ball bearings packed in ordered rhombohedra geometry. It revealed that, an increase in the relative horizontal spacing of balls in the same geometric array had a very significant effect in decreasing the pressure and the effect of ball spacing on pressure drop was more important than that of voidage. Nakayama et al. (1995) studied the flow within a three-dimensional spatially periodic array of cubic blocks with different flow directions. They found that, the macroscopic correlation form of pressure drop obtained by their model was similar to that of Ergun equation, but the value of inertial coefficient in the correlation was much lower. Calis et al. (2001) and Romkes et al. (2003) investigated the flow and heat transfer characteristics in composite structured packed beds of spheres with CFD and experimental methods. Five different packing forms were studied. The computational results agreed well with the experiment results. The results showed that, the effects of packing forms on macroscopic flow and heat transfer characteristics were remarkable. By using composite structured packings, the pressure drop could be greatly reduced. The traditional correlations for flow and heat transfer obtained from random packings were unavailable for composite structured packings. Considering four different periodically repeating arrangements of particles, Gunjal et al. (2005) studied the flow and heat transfer in an array of spheres with unit-cell approach. When in turbulent flow region, the Ergun equation (Ergun, 1952) overpredicts the drag coefficient and Wakao equation (Wakao and Kaguei, 1982) overpredicts the Nusselt number of particle to fluid. Furthermore, Larachi et al. (2003) and Petre et al. (2003) developed a combined mesoscale–microscale predictive approach to apprehend the aerodynamic macroscale phenomena in structured packings. They advocated CFD as a successful, rapid and economic tool for design and optimization, in terms of energy dissipation, of new structured packing shapes. Similar studies for structured packed beds were also presented by Suekane et al. (2003), Nijemeisland and Dixon (2001) and Lee et al. (2007).

All these studies demonstrate that, CFD method is reliable for modeling flow and heat transfer phenomena inside packed beds of particles. Not only local behavior but also macroscopic characteristics of flow and heat transfer are significantly affected by the internal structural properties of packed beds. The pressure drops can be greatly reduced by using structured packings and the traditional correlations are questionable for formulating flow and heat transfer performances in structured packed beds.

According to these studies, we can believe that, with proper selection of packing form and particle shape, the overall heat transfer performances of packed beds would be improved. In order to give a comprehensive understanding of the transport processes in structured packed beds and optimize the overall heat transfer performances, the flow and heat transfer inside small pores of novel packings, such as non-uniform packing and packings of ellipsoid particles, are studied in this paper. According to authors' knowledge, almost no attentions have been paid to such packings yet and some new transport phenomena would be obtained. Three-dimensional Navier–Stokes and energy equations are solved by using commercial code CFX10. The effects of Reynolds number, packing form and particle shape are studied in detail.

2. Physical model and computational method

2.1. Physical model and dimensions

As shown in Fig. 1a, the packed bed consisting of large number of particles (more than 1000) is orderly stacked in a square channel, where the ratio of channel height to particle diameter (N) is larger than 10. The channel walls are adiabatic and the temperature of particle surfaces is kept at T_p. Air is used as the cold fluid and the inlet temperature and velocity are kept at T_0 and u_0, respectively. For current computational condition, direct simulation of flow and heat transfer for the entire packed bed with so large number of particles is still infeasible. Therefore, representative packed channel with appropriate boundary conditions is selected for present study (see Fig. 1b). The computational domain consists of inlet block, packed channel and outlet block. The packed channel is composed of 8 packed cells to guarantee periodically developed flow and heat transfer inside. The symmetry boundary conditions are adopted for top, bottom and side walls and the outlet flow and heat transfer are considered to be fully developed. As shown in Fig. 2, six different kinds of packed cells, including three kinds of packing forms (simple cubic, body center cubic and face center cubic packing) and three kinds of particle shapes (spherical, flat ellipsoidal and long ellipsoidal particle), are selected for investigating the effects of configuration. The body center packing is divided into uniform and non-uniform packings. The non-uniform body center packing is composed of eight big particles at eight corners and one small particle at body center, where eight big particles contact with each other and the small particle contacts with all big particles. Based on these packed cells, six different packed channels are also constructed as presented in Fig. 3, where each packed channel is composed of 8 packed cells. The physical dimensions of computational domain and different packed cells are presented in Table 1.

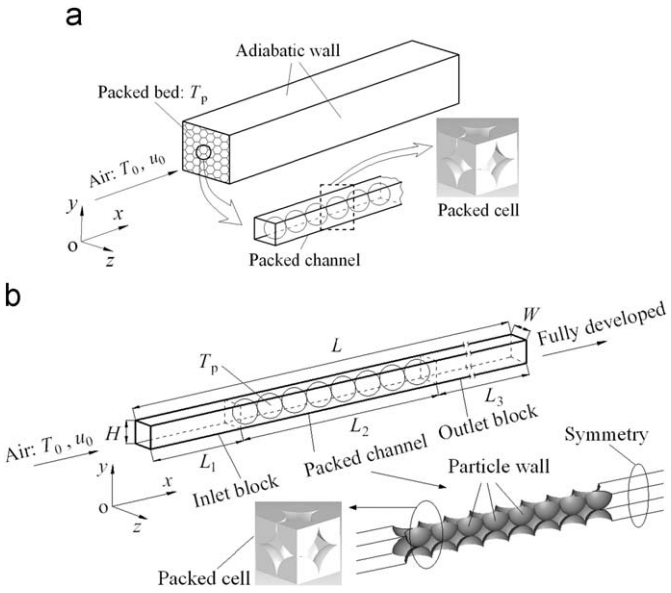

Fig. 1. Physical model: (a) structured packed bed and (b) representative computational domain.

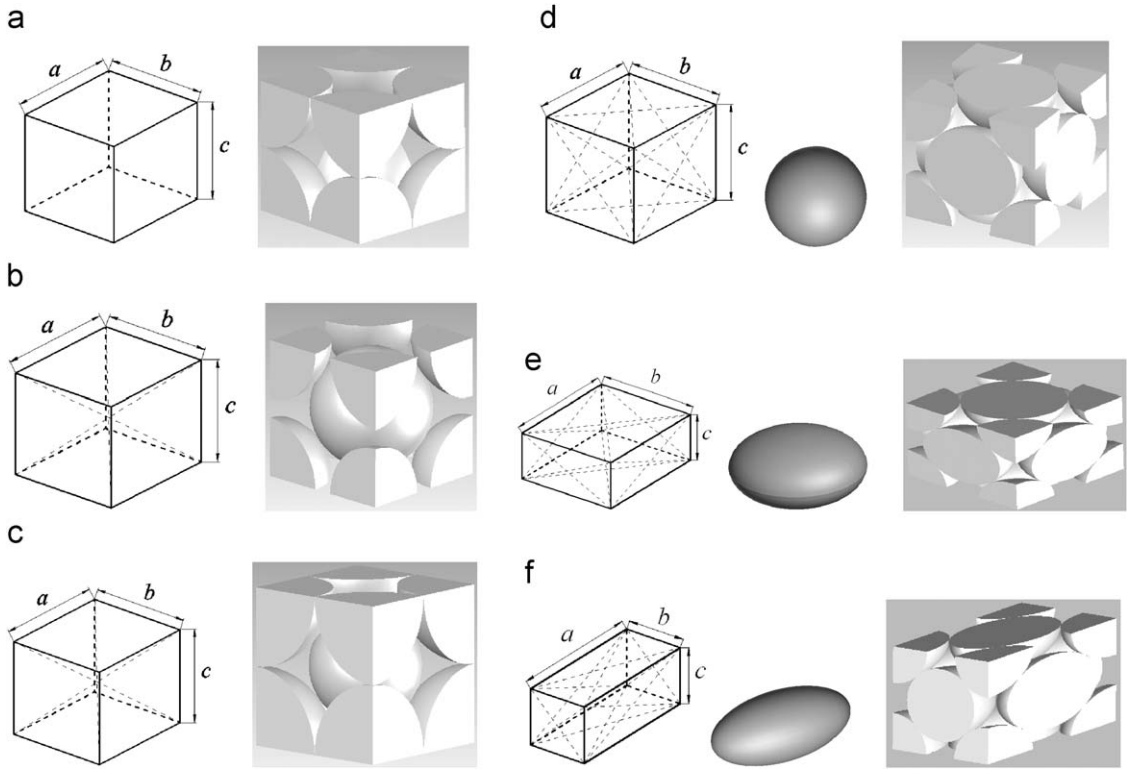

Fig. 2. Different packed cells:(a) SC (Sphere);(b) BCC (Uniform sphere);(c) BCC-1 (Non-uniform sphere);(d) FCC (Sphere);(e) FCC-1 (Flat ellipsoid) and (f) FCC-2 (Long ellipsoid).

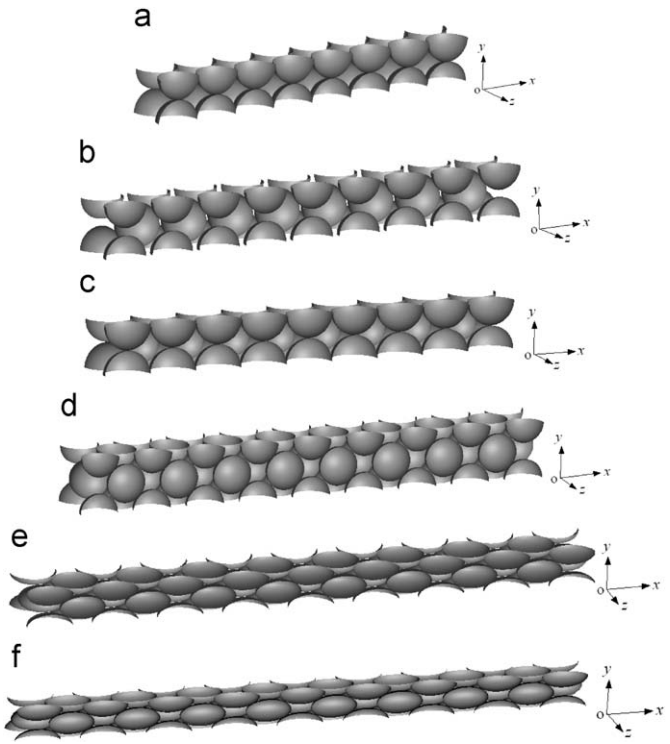

Fig. 3. Different packed channels: (a) SC (Sphere);(b) BCC (Uniform sphere);(c) BCC-1 (Non-uniform sphere);(d) FCC (Sphere);(e) FCC-1(Flat ellipsoid) and (f) FCC-2 (Long ellipsoid).

2.2. Governing equations and computational methods

The flow in the computational domain is considered to be incompressible and steady. Three-dimensional Navier–Stokes and energy equations are employed for the computation. The RNG k–ε turbulence model and scalable wall function are adopted for internal turbulent flow when $Re > 300$. The RNG k–ε turbulence model is applicable to the small-scale eddies, which are independent of the larger-scale phenomena that create them, and it is more suitable for modeling turbulent flow in complex geometries (Yakhot and Orszag, 1986; Nijemeisland and Dixon, 2004). Because the computational domain is symmetrical according to y and z axis, only 1/4 part of the computational domain is finally used for the simulation. Furthermore, since particle surfaces are assumed to be isothermal, the heat transfer inside solid particles is not considered. The conservation equations for mass, momentum, and energy are as follows:

Continuity:

$$\nabla \cdot \vec{V} = 0 \tag{1}$$

Momentum:

$$\rho_f(\vec{V} \cdot \nabla \vec{V}) = -\nabla p + \nabla \cdot [(\mu_f + \mu_t)(\nabla \vec{V} + (\nabla \vec{V})^T)] \tag{2}$$

Energy:

$$\rho_f(\vec{V} \cdot \nabla T) = \nabla \cdot \left[\left(\frac{k_f}{c_p} + \frac{\mu_t}{\sigma_T}\right)(\nabla T)\right] \tag{3}$$

The transport equations for RNG k–ε model are as follows (CFX 10, 2005):

$$\begin{cases} k: \quad \rho_f(\vec{V} \cdot \nabla k) = \nabla \cdot \left[\left(\mu_f + \dfrac{\mu_t}{\sigma_k}\right)\nabla k\right] + P_k - \rho_f \varepsilon \\ \varepsilon: \quad \rho_f(\vec{V} \cdot \nabla \varepsilon) = \nabla \cdot \left[\left(\mu_f + \dfrac{\mu_t}{\sigma_\varepsilon}\right)\nabla \varepsilon\right] + \dfrac{c_{\varepsilon 1}\varepsilon}{k} P_k - c_{\varepsilon 2}\rho_f \dfrac{\varepsilon^2}{k} \end{cases} \tag{4}$$

Table 1
Geometry parameters for physical models.

Packing model	a (mm)	$b(W)$ (mm)	$c(H)$ (mm)	L_1 (mm)	L_2 (mm)	L_3 (mm)	ϕ	d_p (mm)	d_h (mm)
SC (sphere)	12.12	12.12	12.12	30	96.96	80	0.492	12.00	7.75
BCC (uniform sphere)	14.00	14.00	14.00	30	123.96	80	0.340	12.00	4.12
BCC-1 (non-uniform sphere)	12.12	12.12	12.12	30	108.96	80	0.293	10.64	3.00
FCC (sphere)	17.14	17.14	17.14	30	149.12	80	0.282	12.00	3.14
FCC-1 (flat ellipsoid)	21.58	21.58	10.79	30	187.73	80	0.281	12.00	2.86
FCC-2 (long ellipsoid)	27.21	13.61	13.61	30	236.72	80	0.282	12.00	2.92

where P_k is the shear production of turbulence; μ_t is the turbulent viscosity; $c_{\varepsilon 1}$ and $c_{\varepsilon 2}$ are the turbulence model constants in ε equation; σ_T,σ_k and σ_ε are the Prandtl numbers in energy, k and ε equations. Their definitions and values are as follows:

$$P_k = \mu_t \cdot (\nabla\vec{V} + (\nabla\vec{V})^T) : \nabla\vec{V};$$

$$\mu_t = \rho_f c_\mu \frac{k^2}{\varepsilon} (c_\mu = 0.085);$$

$$c_{\varepsilon 1} = 1.42 - f_\eta \left(f_\eta = \frac{\eta(1-\eta/4.38)}{1+0.012\eta^3}, \eta = \frac{P_k}{\rho_f c_\mu \varepsilon} \right);$$

$$c_{\varepsilon 2} = 1.68; \sigma_T = 1.0; \sigma_k = \sigma_\varepsilon = 0.718.$$

Boundary conditions:

$$\begin{cases} x = 0 & T = T_0,\ u = u_0,\ v = w = 0,\ k = k_0,\ \varepsilon = \varepsilon_0 \\ x = L & \dfrac{\partial T}{\partial x} = \dfrac{\partial u}{\partial x} = \dfrac{\partial v}{\partial x} = \dfrac{\partial w}{\partial x} = \dfrac{\partial k}{\partial x} = \dfrac{\partial \varepsilon}{\partial x} = 0 \\ y = 0,\ H/2 & \dfrac{\partial T}{\partial y} = \dfrac{\partial u}{\partial y} = \dfrac{\partial w}{\partial y} = \dfrac{\partial k}{\partial y} = \dfrac{\partial \varepsilon}{\partial y} = 0,\ v = 0 \\ z = 0,\ W/2 & \dfrac{\partial T}{\partial z} = \dfrac{\partial u}{\partial z} = \dfrac{\partial v}{\partial z} = \dfrac{\partial k}{\partial z} = \dfrac{\partial \varepsilon}{\partial z} = 0,\ w = 0 \\ \text{Particle walls} & T = T_p,\ u = v = w = k = \varepsilon = 0 \end{cases}$$

The governing equations are solved by using commercial code CFX10 and the convective term in momentum equations is discretized with high resolution scheme. The continuity and momentum equations are solved together with coupled algorithm based on finite control volume method. For convergence criteria, the relative variations of the temperature and velocity between two successive iterations are demanded to be smaller than the previously specified accuracy levels of 1.0×10^{-6}.

3. Grid independence test and model validation

Before proceeding further, the grid used for present study is checked at first. The SC packing with uniform spheres is selected for the test, as shown in Fig. 2a. Both laminar (Re=10) and turbulent (Re=1000) flows are studied. As shown in Fig. 4, the unstructured grids with tetrahedral elements are used and the grids are intensified on particle walls. In order to avoid generating poor quality meshes at contact points between particles, the particles are stacked with very small gaps (1% of d_p) instead of contact points between each other. According to the studies of Calis et al. (2001) and Nijemeisland and Dixon (2001), these gaps have very small influence on the flow and heat transfer ($<0.5\%$). The total numbers of grid elements vary from 389 247 to 819 694, and the computational results are shown in Table 2, where the Richardson extrapolation approach (Celik and Zhang, 1995) is also adopted to get higher order accuracy results. It shows that, the grid with total element number of 625 795 is good enough for both laminar and turbulent flows, where the maximum length of the grid element is less than 1 mm for central flow and 0.2 mm for near wall flow regions. For turbulent flow, with scalable wall function method, the value of dimensionless distance of the wall grid elements is of $y^+ > 11.06$. Therefore, similar grids to that of the test case are finally employed for the following studies. The total numbers of grid elements for different packings are listed in Table 3.

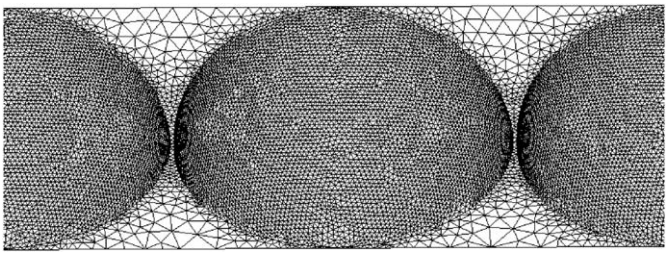

Fig. 4. Part of computational grid for SC (Sphere) packing model.

Furthermore, in order to validate the reliability and accuracy of present computational models and methods, similar problem reported by Calis et al. (2001) and Romkes et al. (2003) are restudied in this section. For the selected problem, as shown in Fig. 5, eight uniform spheres are orderly stacked within a square channel, where the ratio of channel height to particle diameter (N) equals 1. The channel walls are adiabatic and the temperature of particle surfaces is kept at T_p. Air is used as the cold fluid and the inlet temperature and velocity are kept constant. The computational model and method used for this problem are similar to those presented in Section 2. The predicted friction factor (f) and Nusselt number of particles to fluid (Nu_{sf}) are compared with those reported in the above references (Calis et al., 2001; Romkes et al., 2003) in Fig. 6. The average deviation of f is less than 5% and the average deviation of Nu_{sf} is less than 10%. This indicates that, the computational models and methods presented in this study are reliable and capable of modeling flow and heat transfer phenomena inside packed beds of particles.

4. Results and discussion

4.1. Basic hydrodynamic and heat transfer correlations

The macroscopic hydrodynamic and heat transfer performances in packed beds are usually formulated by traditional correlations as follows (Ergun, 1952; Wakao and Kaguei, 1982):

$$\frac{\Delta p}{\Delta x} = f \cdot \frac{1}{2}\rho_f \left(\frac{|\vec{V}_D|}{\phi} \right)^2 \frac{1}{d_h} \left(f = \frac{c_1}{Re} + c_2 \right) \tag{5}$$

$$Nu_{sf} = \frac{h_{sf} \cdot d_p}{k_f} = a_1 + a_2 Pr^{1/3} \cdot Re^n \cdot \left(\frac{d_p}{d_h}\phi \right)^n \tag{6}$$

where f is the friction factor. c_1, c_2 are the model constants in friction factor correlation, with c_1=133 and c_2=2.33 in Ergun equation (Ergun, 1952). h_{sf} is the heat transfer coefficient of

Table 2
Total pressure drop and heat quantity for SC packing (sphere) with different grids (Pr=0.7, Re=10, 1000).

	Grid (total elements)				Richardson extrapolation
	389 247	513 393	625 795	819 694	
$\Delta p_{total,Re=10}$/Pa	0.0489	0.0527	0.0539	0.0546	0.0556
$Q_{total,Re=10}$/W	0.0167	0.0175	0.0179	0.0182	0.0186
$\Delta p_{total,Re=1000}$/Pa	33.125	35.110	36.261	36.625	37.132
$Q_{total,Re=1000}$/W	0.864	0.897	0.915	0.930	0.951

Table 3
Computational grids for different packing models.

Packing model	SC (sphere)	BCC (uniform sphere)	BCC-1 (non-uniform sphere)	FCC (sphere)	FCC-1 (flat ellipsoid)	FCC-2 (long ellipsoid)
Grid (total elements)	625795	1263 527	885603	2312 012	2444 331	2373 971

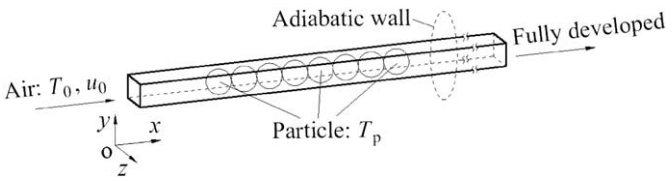

Fig. 5. Physical model used by Calis et al. (2001) and Romkes et al. (2003).

particle to fluid. a_1, a_2 and n are the model constants in heat transfer equation, with a_1=2.0, a_2=1.1 and n=0.6 in Wakao equation (Wakao and Kaguei, 1982). The Reynolds number (Re), pore scale hydraulic diameter (d_h) and equivalent particle diameter (d_p) are defined as follows:

$$Re=\frac{\rho_f(|\vec{V}_D|/\phi)d_h}{\mu_f};\ d_h=4\frac{\phi}{1-\phi}\left(\frac{V_p}{A_p}\right)_{cell};\ d_p=2\left(\frac{3V_p}{4\pi}\right)^{1/3} \tag{7}$$

where $\vec{V}_D$ is the Darcy velocity vector; ϕ is the porosity; V_p is the particle volume; A_p is the area of particle surface. The subscript "cell" means the value is obtained within packed cell.

Furthermore, the flow in packed beds can be considered as flow in porous media, the macroscopic hydrodynamics can be modeled by Forchheimer extended Darcy model (Nield and Bejan, 2006) as follows:

$$-\frac{dp}{dx}=\frac{1}{\rho_f}\frac{\mu_f}{K}\vec{V}_D+\frac{c_F}{\sqrt{K}}|\vec{V}_D|\vec{V}_D \tag{8}$$

Compare Eq. (8) with Eq. (5), the permeability (K) and the Forchheimer coefficient (c_F) can be defined as follows:

$$K=\frac{d_h^2\cdot\phi}{c_1/2};\ c_F=\frac{c_2/2}{\sqrt{c_1/2}}\cdot\phi^{-3/2}. \tag{9}$$

In the present study, the microscopic results obtained in the 5th to 7th packed cells are integrated and averaged to extract the macroscopic results, where the periodic flow and heat transfer are formed inside. The macroscopic pressure drop ($\Delta p/\Delta x$), heat transfer coefficient (h_{sf}) and overall heat transfer efficiency (γ) are

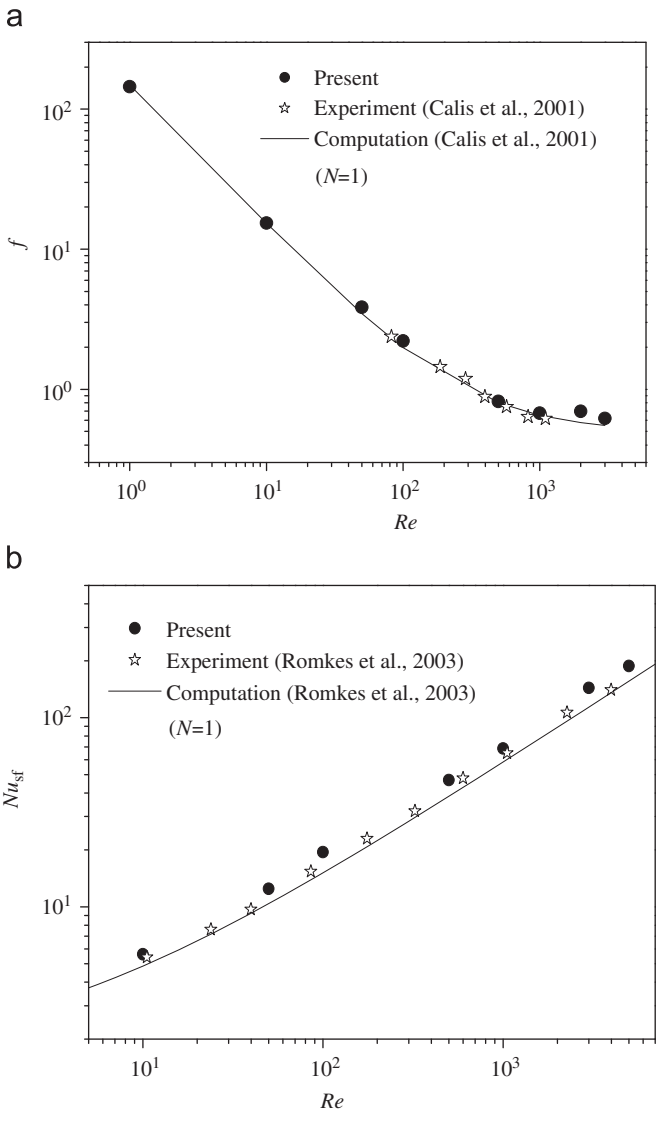

Fig. 6. Variations of friction factor and Nusselt number of particle to fluid: (a) f and (b) Nu_{sf}.

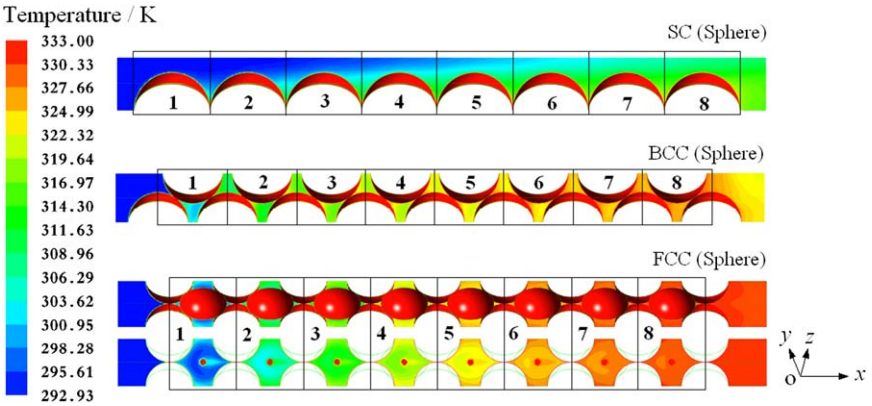

Fig. 7. Temperature fields in central diagonal cross-sections of different packings with spherical particles (T_0=293 K, T_p=333 K, Pr=0.7, Re=1000).

defined as follows:

$$\frac{\Delta p}{\Delta x}=\frac{1}{3}\sum_{\text{cell5}}^{\text{cell7}}\frac{1}{(x_{\text{out}}-x_{\text{in}})A_{\text{in}}}\int\int_{A_{\text{in}}}(p_{\text{in}}-p_{\text{out}})dA;$$
$$h_{\text{sf}}=\frac{1}{3}\sum_{\text{cell5}}^{\text{cell7}}\frac{\rho_f c_p\int\int_{A_{\text{in}}}u(T_{\text{f,out}}-T_{\text{f,in}})dA}{A_p(T_p-\overline{T}_f)};\gamma=h_{sf}/\Delta p \tag{10}$$

where Δp and $\overline{T}_f$ are the average pressure drop and temperature of fluid in packed cell, respectively, and their definitions are as follows:

$$\Delta p=\frac{1}{3}\sum_{\text{cell5}}^{\text{cell7}}\frac{1}{A_{\text{in}}}\int\int_{A_{\text{in}}}(p_{\text{in}}-p_{\text{out}})dA;$$
$$\overline{T}_f=\left(\frac{1}{2}\frac{\int\int_{A_{\text{in}}}u(T_{\text{f,out}}+T_{\text{f,in}})dA}{\int\int_{A_{\text{in}}}udA}\right)_{\text{cell}} \tag{11}$$

where the subscript "in" and "out" means the inlet and outlet sections of packed cell, respectively.

4.2. The effect of packing form

Firstly, the effect of packing form is examined and three different kinds of packing forms are studied in this section (SC, BCC and FCC packings with uniform spheres, see Fig. 2a, b and d). The Reynolds number (Re) is varying from 1 to 5000 with Pr=0.7, T_0=293 K and T_p=333 K.

In order to produce periodically developed flow and heat transfer in packed channels, each packed channel is composed of 8 packed cells. The temperature distributions in central diagonal cross-sections of different packings are shown in Fig. 7. It shows that, the fluid temperature in the FCC packed channel increases most quickly along main flow direction. The average temperatures of fluid in the 6th packed cells of SC, BCC and FCC packings are 308, 317 and 327 K, respectively, which indicates that, the heat transfer of the FCC packing would be the highest and it would be the lowest for the SC packing. The configuration of the FCC packing is the most compact and its surface area-to-volume ratio is the highest, which leads to the best heat transfer performance. The local streamline distributions in the 6th and 7th packed cells of different packings are shown in Fig. 8, where the periodically developed flows are formed inside. Under the same Reynolds number, the fluid velocity in the FCC packed cells is the highest and it is the lowest for the SC packing. Large vortices are formed in the SC packed cells, and such vortices become smaller in the BCC

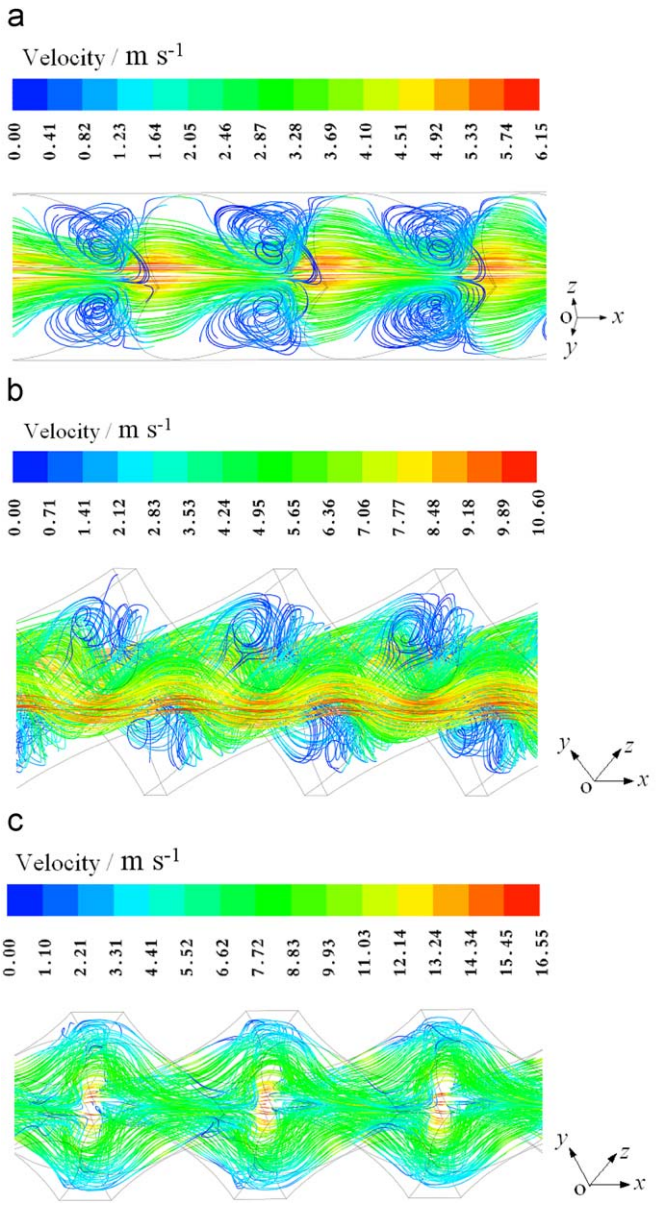

Fig. 8. Local streamline distributions in different packings with spherical particles (Pr=0.7, Re=1000): (a) SC (Sphere) (b) BCC (Sphere) and (c) FCC (Sphere).

and FCC packed cells as porosity decreases. Therefore, the pressure drop of the FCC packing would be the highest because of the lowest porosity, but the local tortuosity of the SC packing would be the highest because of large vortices inside.

The variations of pressure drop ($\Delta p/\Delta x$) and friction factor (f) with Reynolds numbers are shown in Fig. 9. In Fig. 9a, it shows that, as Re increases, the pressure drops of different packings increase. The pressure drop of the FCC packing is the highest and it is the lowest for the SC packing, which agrees well with the analysis of local flow variations. When Re is small ($Re < 10$), the viscosity effects dominate and the predicted pressure drops of structured packings agree well with those obtained by the Ergun equation. As Re increases ($Re > 10$), the inertial effects are increasing and become dominant, and the Ergun equation overpredict the pressure drops for structured packings. These results show that, the hydrodynamics of structured packings and random packings are quite different. The tortuosities of structured packings are much lower and the pressure drops would be greatly reduced. In Fig. 9b, it shows that, as Re increases, the friction factors decrease at first and then keep constant when $Re > 3000$, which agrees well with traditional studies. When $Re < 10$, the friction factors of different packings are almost same. When $Re > 10$, the deviations are becoming large. The friction factor of the SC packing is the highest and it is the lowest for the FCC packing. The model constants c_1, c_2 in friction factor f correlation (in Eq. (5)) are obtained with non-linear fitting method and the average fitting deviation is less than 5%. The predicted values of c_1, c_2 are compared in Table 4. For different structured packings, the values of c_1 are similar, while the values of c_2 are quite different, which is the highest for the SC packing and the lowest for the FCC packing. This confirms that, the tortuosity of the SC packing is the highest and it is the lowest for the FCC packing.

The variations of Nusselt number (Nu_{sf}) and overall heat transfer efficiency (γ) of particle to fluid with Reynolds numbers are shown in Fig. 10. In Fig. 10a, it shows that, as Re increases, the Nusselt numbers of different packings increase. The value of Nu_{sf}

Table 4
Predicted values of c_1, c_2 (sphere).

Packing model	ϕ	d_h (mm)	c_1	c_2
SC (sphere)	0.492	7.75	143.88	0.882
BCC (sphere)	0.340	4.12	129.81	0.374
FCC (sphere)	0.282	3.14	164.12	0.297
Random (Ergun, 1952)	–	–	133	2.33

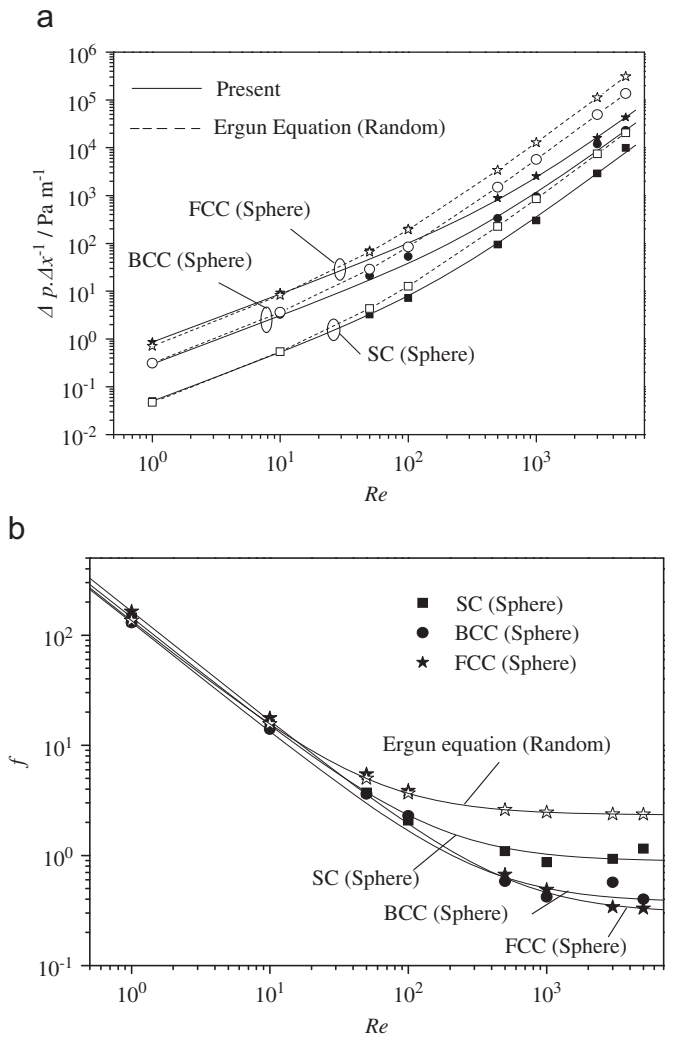

Fig. 9. Variations of pressure drops and friction factors for different packing forms (sphere): (a) $\Delta p.\Delta x^{-1}$/Pa m^{-1} and (b) f.

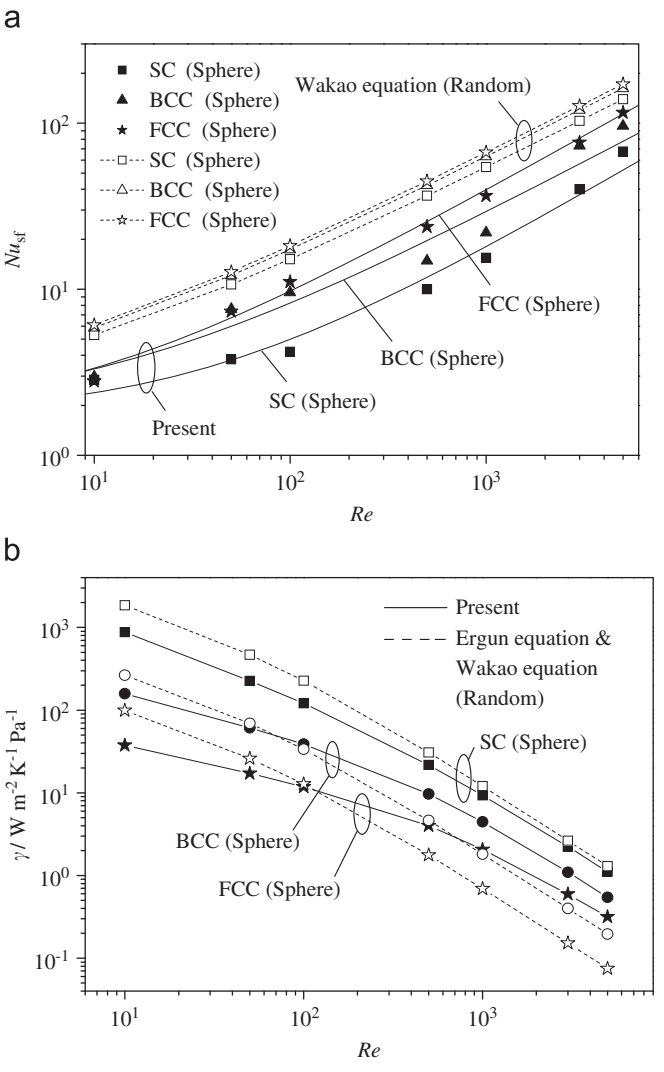

Fig. 10. Variations of Nusselt numbers and overall heat transfer efficiencies of particle to fluid for different packing forms (sphere): (a) Nu_{sf} and (b) γ/Wm^{-2}K^{-1} Pa^{-1}.

for the FCC packing is the highest and it is the lowest for the SC packing, which agrees well with the analysis of local temperature variations. The Wakao equation is found to overpredict Nu_{sf} for structured packings. The model constants a_1, a_2 and n in Nu_{sf} correlation (in Eq. (6)) are obtained with non-linear fitting method and the average fitting deviation is less than 10%. The predicted values of a_1, a_2 and n are compared in Table 5. For different structured packings, the values of a_1 and n are similar; while the values of a_2 are quite different, which is the highest for the FCC packing and the lowest for the SC packing. In Fig. 10b, it shows that, as Re increases, the overall heat transfer efficiencies of different packings decreases. The value of γ for the SC packing is the highest and it is the lowest for the FCC packing. These results indicate that, high heat transfer performance of the FCC packing model is obtained at cost of high pressure drop, and the overall heat transfer performance is low. With the same physical parameters, the overall heat transfer efficiencies of the BCC and FCC packings are much higher than that of random packings when $Re > 100$, however, the overall heat transfer efficiency of the SC packing is lower than that of random packing. Therefore, for high porosity case, the random packing is recommended, while for low porosity case, the structured packing forms, such as BCC and FCC packings are recommended for applications.

4.3. The effect of particle shape

In this section, the effect of particle shape is investigated. Three different kinds of particles are compared, including spherical, flat ellipsoidal and long ellipsoidal particles. Since the heat transfer capacity of the FCC packing is the highest, this packing form is selected for present study (FCC (sphere), FCC-1 (flat ellipsoid) and FCC-2 (long ellipsoid) packings, see Fig. 2d–f). The Reynolds number (Re) is varying from 1 to 5000 with Pr=0.7, T_0=293 K and T_p=333 K.

The temperature distributions in the central diagonal cross-sections of different particle models are shown in Fig. 11. It shows that the temperature distributions of different particle models are similar under the same packing form. Therefore, the heat transfer performances of different particle models may be close under the same packing form. The local streamline distributions in the 6th packed cells of different particle models are shown in Fig. 12. It shows that, under the same Reynolds number, the fluid velocity in the FCC packed cell is the highest and it is the lowest for the FCC-2 model. For the intrinsic characteristics of particle shape, the tortuosity of the FCC model is the highest and it is the lowest for the FCC-2 model. These results indicate that, under the same packing form, the tortuosity and the pressure drop would be reduced with proper selection of particle shape, and the overall heat transfer efficiency may be improved.

Table 5
Predicted values of a_1, a_2 and n (sphere).

Packing model	ϕ	d_h (mm)	d_p (mm)	a_1	a_2	n
SC (sphere)	0.492	7.75	12.00	1.73	0.16	0.70
BCC (sphere)	0.340	4.12	12.00	1.80	0.40	0.63
FCC (sphere)	0.282	3.14	12.00	1.60	0.41	0.67
Random (Wakao and Kaguei, 1982)	–	–	–	2.00	1.10	0.60

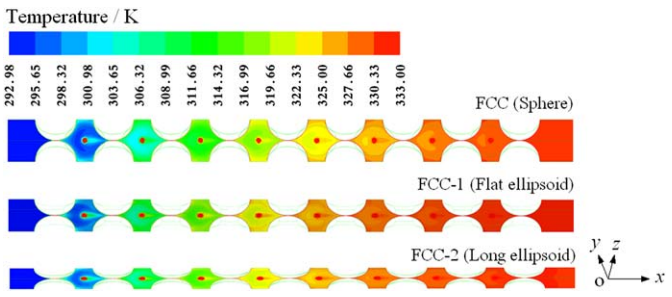

Fig. 11. Temperature fields in central diagonal cross-sections of FCC packings with different particles (T_0=293 K, T_p=333 K, Pr=0.7, Re=1000).

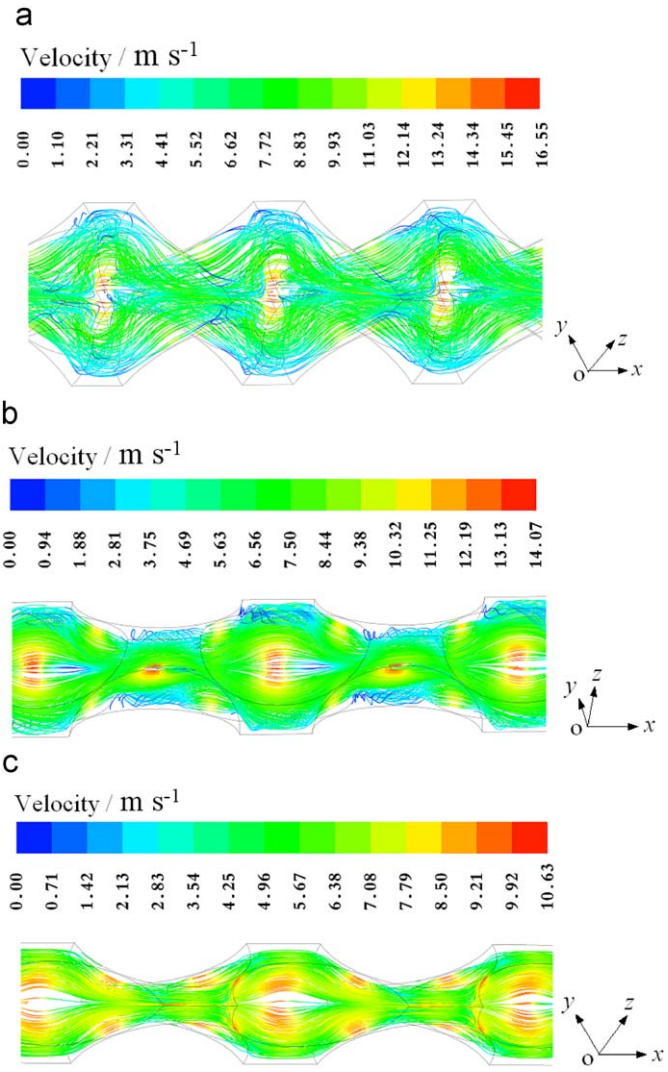

Fig. 12. Local streamline distributions in FCC packings with different particles (Pr=0.7, Re=1000): (a) FCC (Sphere); (b) FCC-1 (Flat ellipsoid) and (c) FCC-2 (Long ellipsoid).

The variations of pressure drop ($\Delta p/\Delta x$) and friction factor (f) with Reynolds numbers are shown in Fig. 13. In Fig. 13a, it shows that, the pressure drops of the FCC and FCC-1 models are similar, which are higher than those of the FCC-2 model. The Ergun equation is found again to overpredict the pressure drops of different particle models. With proper selection of particle shapes, the pressure drop can be reduced with the same packing form. In Fig. 13b, it shows that, as Re increases, the friction factors of different particle models decrease at first and then keep constant. The friction factor of the FCC model is the highest and it is the lowest for the FCC-2 model. The predicted values of c_1, c_2 for friction factor correlations are compared in Table 6, which are the

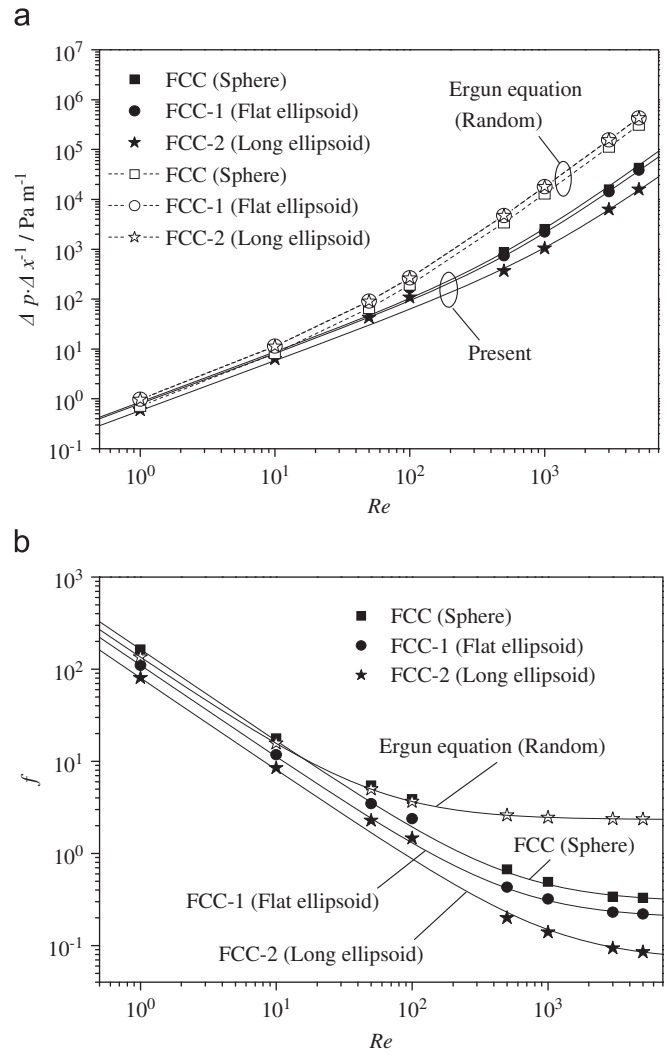

Fig. 13. Variations of pressure drops and friction factors for FCC packings with different particles: (a) $\Delta p.\Delta x^{-1}$/Pa m^{-1} and (b) f.

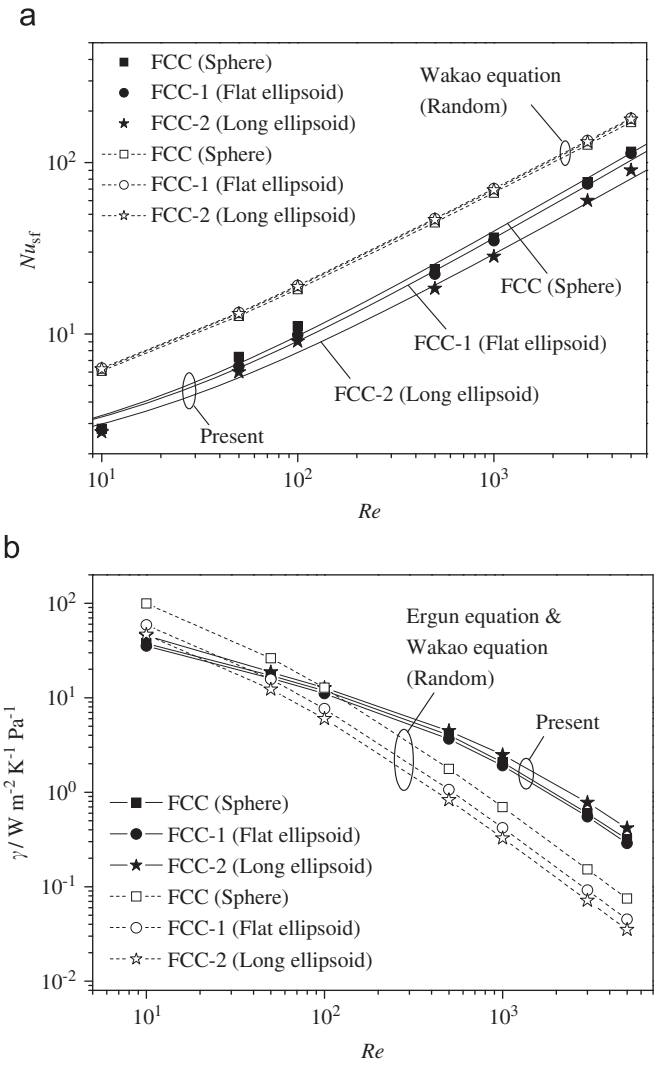

Fig. 14. Variations of Nusselt numbers and overall heat transfer efficiencies of particle to fluid for FCC packings with different particles: (a) Nu_{sf} and (b) γ/Wm^{-2} K^{-1}Pa^{-1}.

Table 6
Predicted values of c_1, c_2 (FCC).

Packing model	ϕ	d_h (mm)	c_1	c_2
FCC (sphere)	0.282	3.136	164.12	0.297
FCC-1 (flat ellipsoid)	0.281	2.855	110.43	0.198
FCC-2 (long ellipsoid)	0.282	2.915	80.35	0.069
Random (Ergun, 1952)	–	–	133	2.33

highest for the FCC model and the lowest for the FCC-2 model. This confirms that, the tortuosity for the FCC model is the highest and it is the lowest for the FCC-2 model.

The variations of Nusselt number (Nu_{sf}) and overall heat transfer efficiency (γ) of particle to fluid with Reynolds numbers are shown in Fig. 14. In Fig. 14a, it shows that, the Nusselt numbers of the FCC and FCC-1 models are similar, which are higher than those of the FCC-2 model. The Wakao equation is found again to overpredict Nu_{sf} for different particle models. The predicted values of a_1, a_2 and n for Nu_{sf} correlations are compared in Table 7. For different particle models, the values of a_1 and n are close to those of Wakao equation, while the values of a_2 are much lower. In Fig. 14b, it shows that, as Re increases, the overall heat transfer efficiencies of different particle models decrease. With the same physical parameters, the values of γ for different particle models are much higher than those of random packings when $Re > 100$. The overall heat transfer efficiencies of the FCC and FCC-1 models are close, which are lower than that of the FCC-2 model. This confirms that, with the same packing form, the overall heat transfer performance can be improved with proper selection of particle shape. The overall heat transfer performance of the long ellipsoidal particle model (FCC-2) is the highest and this particle shape is recommended for applications.

Table 7
Predicted values of a_1, a_2 and n (FCC).

Packing model	ϕ	d_h (mm)	d_p (mm)	a_1	a_2	n
FCC (sphere)	0.282	3.136	12.00	1.60	0.40	0.67
FCC-1 (flat ellipsoid)	0.281	2.855	12.00	1.70	0.34	0.67
FCC-2 (long ellipsoid)	0.282	2.915	12.00	1.60	0.32	0.65
Random (Wakao and Kaguei, 1982)	–	–	–	2.00	1.10	0.60

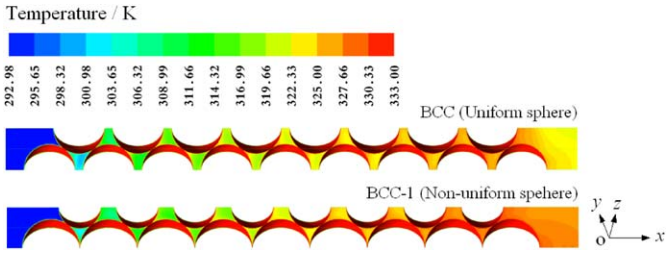

Fig. 15. Temperature fields in central diagonal cross-sections for uniform and non-uniform packings with spherical particles (T_0=293 K, T_p=333 K, Pr=0.7, Re=1000).

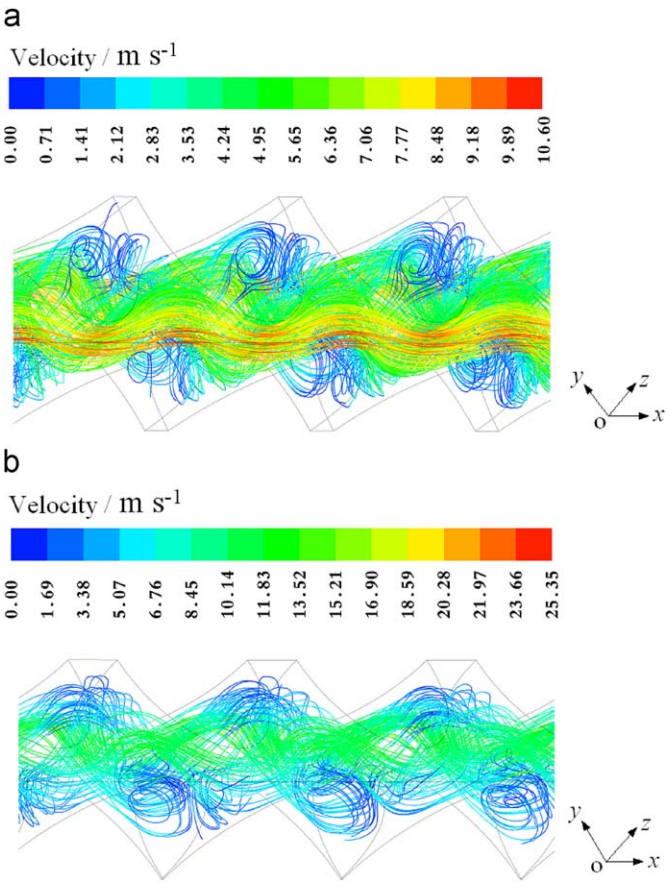

Fig. 16. Local streamline distributions in uniform and non-uniform packings with spherical particles (Pr=0.7, Re=1000): (a) BCC (Uniform sphere) and (b) BCC-1 (Non-uniform sphere).

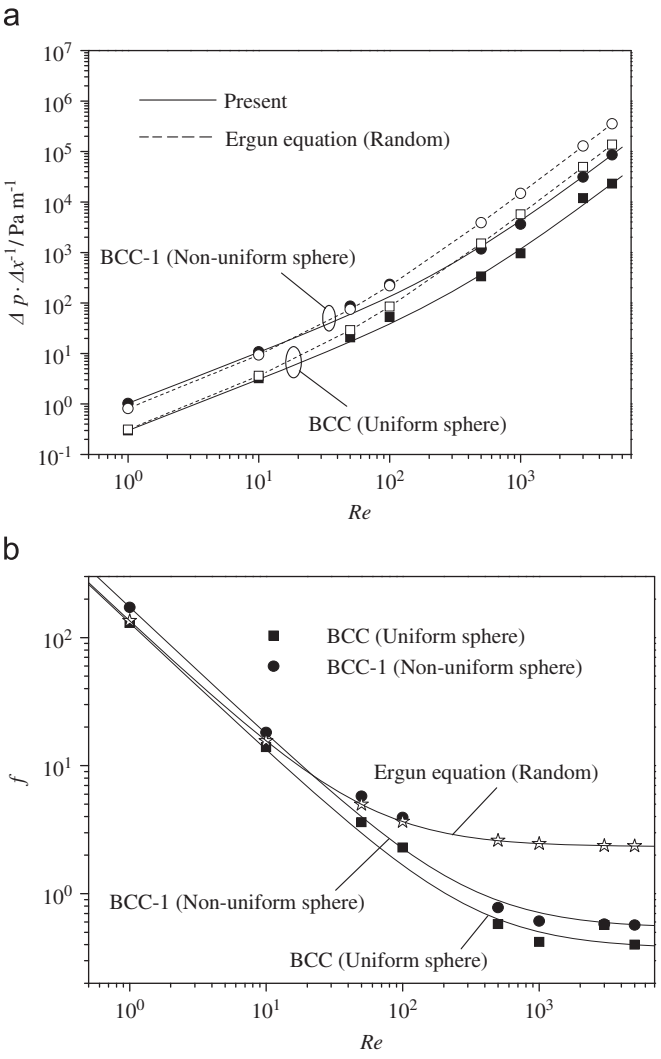

Fig. 17. Variations of pressure drops and friction factors for uniform and non-uniform packings with spherical particles: (a) $\Delta p.\Delta x^{-1}$/Pa m^{-1} and (b) f.

4.4. *Performance comparison for uniform and non-uniform packing models*

Finally, the performances of uniform and non-uniform packings are compared. Since the non-uniform BCC packing form is stable and easy to be constructed, the BCC packing form is adopted for present study (BCC (uniform sphere) and BCC-1(non-uniform sphere) packings, see Fig. 2b and c). The Reynolds number (Re) is varying from 1 to 5000 with Pr=0.7, T_0=293 K and T_p=333 K.

The temperature distributions in central diagonal cross-sections of the BCC and BCC-1 packed channels are shown in Fig. 15. It shows that, the fluid temperature in the BCC-1 packed channel increases more rapidly than that in the BCC packed channel along main flow direction. The average fluid temperatures in the 6th packed cells of the BCC and BCC-1 packings are 317 and 323 K, respectively, which indicates that, the heat transfer of the BCC-1 model would be higher than that of the BCC model. The configuration of the BCC-1 packing is more compact and its surface area-to-volume ratio is higher, which leads to the better heat transfer performance. The local streamline distributions in the 6th and 7th packed cells of the BCC and BCC-1 packings are shown in Fig. 16. With the same Reynolds number, the fluid velocity in the BCC-1 packed cells is much higher than that in the BCC packed cells. There exist pairs of small vortices in the BCC packed cells, but larger vortices are formed in the BCC-1 packed cells. Therefore, both the tortuosity and pressure drop of the BCC-1 packing would be higher.

The variations of pressure drops ($\Delta p/\Delta x$) and friction factors (f) of the BCC and BCC-1 packings are shown in Fig. 17. In Fig. 17a, it shows that, the pressure drop of the BCC-1 packing is higher than that of the BCC packing. The Ergun equation is found to overpredict the pressure drops for both the BCC and BCC-1 packings. Although the pressure drop is higher in the BCC-1 packing, it is still much lower than that in random packings. The variations of friction factors are shown in Fig. 17b and the predicted values of correlation constants c_1, c_2 are compared in

Table 8
Predicted values of c_1, c_2 (BCC).

Packing model	ϕ	d_h (mm)	c_1	c_2
BCC (uniform sphere)	0.340	4.12	129.81	0.374
BCC-1 (non-uniform sphere)	0.293	3.00	172.53	0.540
Random (Ergun, 1952)	–	–	133	2.33

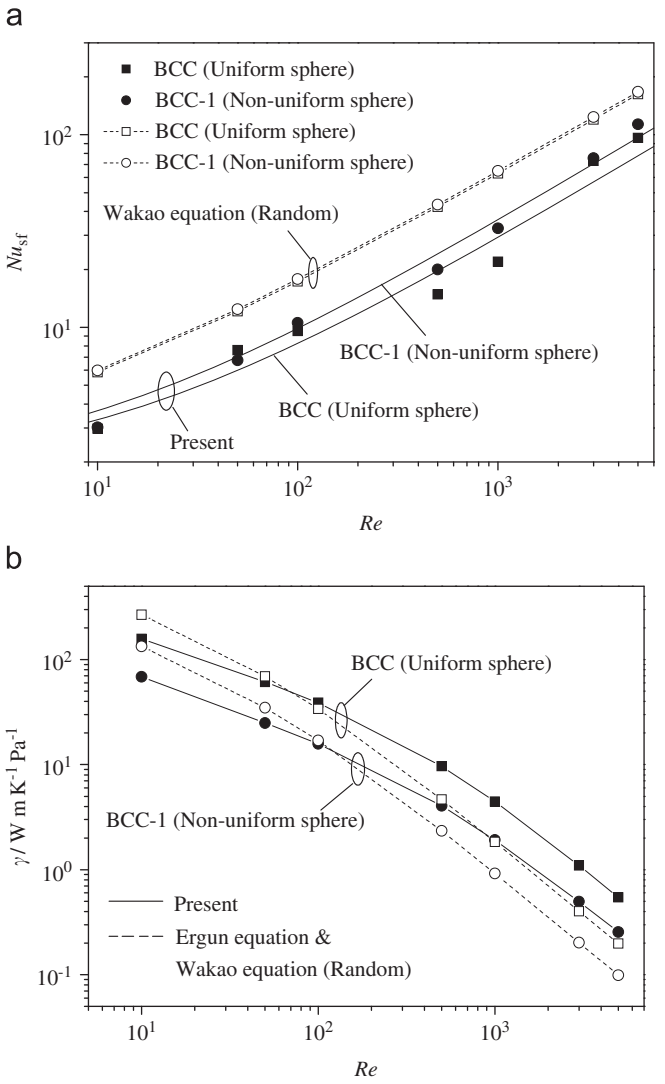

Fig. 18. Variations of particle wall Nusselt numbers and overall heat transfer efficiencies for uniform and non-uniform packings with spherical particles: (a) Nu_{sf} and (b) γ/Wm^{-2}K^{-1}Pa^{-1}.

Table 9
Predicted values of a_1, a_2 and n (BCC).

Packing model	ϕ	d_h (mm)	d_p (mm)	a_1	a_2	n
BCC (uniform sphere)	0.340	4.12	12.00	1.80	0.40	0.63
BCC-1 (non-uniform sphere)	0.293	3.00	10.64	1.80	0.49	0.63
Random (Wakao and Kaguei, 1982)	–	–	–	2.00	1.10	0.60

Table 8. The friction factor and the values of c_1, c_2 for the BCC-1 packing are higher due to the higher tortuosity inside, which agrees well with the analysis of local flow variations.

The variations of Nusselt numbers (Nu_{sf}) and overall heat transfer efficiencies (γ) of particle to fluid for the BCC and BCC-1 packings are shown in Fig. 18. In Fig. 18a, it shows that, the Nusselt number of the BCC-1 packing is higher than that of the BCC packing, which agrees well with the analysis of local temperature variations. The predicted values of a_1, a_2 and n for Nu_{sf} correlations are compared in Table 9. The values of a_1 and n for the BCC-1 packing are the same as those of the BCC packing, while the value of a_2 is higher. In Fig. 18b, it shows that, as Re increases, the overall heat transfer efficiency for both packings decreases. With the same physical parameters, the values of γ for both packings are much higher than those of random packings when $Re > 100$. The overall heat transfer efficiency of the BCC packing is higher than that of the BCC-1 packing. This indicates that, with the same packing form and particle shape, the heat transfer performance can be improved by using non-uniform packing while the overall heat transfer performance of such packing is lower due to its higher pressure drop. Therefore, with the same packing form and same particle shape, the uniform packing form is recommended for applications.

5. Conclusions

A direct simulation of flow and heat transfer process inside small pores of some novel structured packed beds has been carried out in this paper, where the packed beds with ellipsoidal or non-uniform spherical particles are investigated for the first time and some new transport phenomena are obtained. The effects of packing form and particle shape are investigated in detail. The flow and heat transfer performances in uniform and non-uniform packed beds are also compared with each other. The major findings are as follows:

Firstly, it is found that, with proper selection of packing form and particle shape, the pressure drop in structured packed beds can be greatly reduced and the overall heat transfer performance will be improved. The traditional correlations are found to overpredict the pressure drops and Nu_{sf} for all the structured packings, and new correlations of flow and heat transfer are obtained. The forms of these new correlations can fit well with those of traditional correlations, but some model constants, such as c_2 and a_2, are much lower.

Secondly, it is revealed that, both the effects of packing form and particle shape are significant on the flow and heat transfer in structured packed beds

(a) with the same particle shape, the overall heat transfer efficiency of the SC packing is the highest, which is the lowest for the FCC packing. With the same physical parameters, the overall heat transfer efficiencies of the BCC and FCC packings are much higher than those of random packings, while the overall heat transfer efficiency of the SC packing is lower than that of random packing. Therefore, for high porosity case, the random packing is recommended, while for low porosity case, the structured packing forms, such as the BCC and FCC packings are recommended for applications.

(b) with the same packing form, such as FCC packing, the variations of pressure drops and heat transfer performances of the spherical (FCC) and flat ellipsoidal particle (FCC-1) models are similar, which are higher than those of the long ellipsoidal particle model (FCC-2), while the overall heat transfer performance of the FCC-2 model is higher than those of the FCC and FCC-1 models. Furthermore, with the same packing form and particle shape, such as BCC packing with

spheres, the pressure drop and heat transfer of the non-uniform packing (BCC-1) are higher than that of the uniform packing (BCC), while the overall heat transfer performance of the BCC-1 packing is lower. Therefore, with the same packing form, the long ellipsoidal particle and uniform packing models are recommended for applications.

These results would be helpful for further understanding the flow and heat transfer characteristics in structured packed beds and they would also be useful for the optimum design of packed bed reactors.

Notation

a	length of packed cell, m
a_1, a_2	model constants in Nusselt number correlation (in Eq. (6))
A	Area, m^2
b	width of packed cell, m
c	height of packed cell, m
c_1, c_2	model constants in friction factor correlation (in Eq. (5))
c_F	Forchheimer coefficient
c_p	specific heat at constant pressure, $J\,kg^{-1}\,K^{-1}$
$c_{\varepsilon 1}$, $c_{\varepsilon 2}$	model constants in turbulent kinetic energy equation (in Eq. (4))
c_μ	model constant in turbulent viscosity correlation
d_h	pore scale hydraulic diameter, m
d_p	equivalent particle diameter, m
f	friction factor
f_η	RNG k–ε turbulence model coefficient
h_{sf}	heat transfer coefficient of particle to fluid, $W\,m^{-2}\,K^{-1}$
H	height of computational domain, m
K	permeability, m^2
k	turbulent kinetic energy, $m^2\,s^{-2}$
k_f	thermal conductivity of fluid, $W\,m^{-1}\,K^{-1}$
L	total length of computational domain, m
L_1	length of inlet block, m
L_2	length of packed channel, m
L_3	length of outlet block, m
n	model constant in Nusselt number correlation (in Eq. (6))
N	ratio of channel height to particle diameter
Nu_{sf}	Nusselt number of particle to fluid
p	pressure, Pa
P_k	shear production of turbulence, $kg\,m^{-1}\,s^{-3}$
Pr	Prandtl number
Re	Reynolds number
T	temperature, K
u	velocity in x direction, $m\,s^{-1}$
V	volume, m^3
$\vec{V}$	velocity vector, $m\,s^{-1}$
$\vec{V}_D$	Darcy velocity vector, $m\,s^{-1}$
W	width of computational domain, m
x, y, z	coordinate directions, m
y^+	dimensionless wall distance

Greek letters

γ	overall heat transfer efficiency, $W\,m^{-2}\,K^{-1}\,Pa^{-1}$
ε	turbulence dissipation rate, $m^2\,s^{-3}$
η	RNG k–ε turbulence model coefficient
μ	dynamic viscosity, $kg\,m^{-1}\,s^{-1}$
μ_t	turbulent viscosity, $kg\,m^{-1}\,s^{-1}$
ρ	density, $kg\,m^{-3}$
σ_k	Prandtl number in turbulent kinetic energy equation
σ_T	Prandtl number in energy equation
σ_ε	Prandtl number in turbulence dissipation rate equation
ϕ	porosity

Subscripts

0	inlet section of packed channel
cell	value obtained in packed cell
f	Fluid
in	inlet section of packed cell
out	outlet section of packed cell
p	particle

Acknowledgments

We would like to acknowledge financial support for this work provided by the National Natural Science Foundation of China (No. 50806056) and National Defense Science and Technology Key Laboratory Foundation of China (No. 9140C7102010804).

References

Calis, H.P.A., Nijenhuis, J., Paikert, B.C., Dautzenberg, F.M., van den Bleek, C.M., 2001. CFD modelling and experimental validation of pressure drop and flow profile in a novel structured catalytic reactor packing. Chemical Engineering Science 56 (4), 1713–1720.

Caulkin, R., Ahmad, A., Fairweather, M., Jia, X., Williams, R.A., 2007. An investigation of sphere packed shell-side columns using a digital packing algorithm. Computers and Chemical Engineering 31 (12), 1715–1724.

Celik, I., Zhang, W.M., 1995. Calculation of numerical uncertainty using Richardson extrapolation: application to some simple turbulent flow calculations. Journal of Fluids Engineering 117 (3), 439–445.

CFX 10. User guide. 2005. CFX Inc., Florida.

Ergun, S., 1952. Fluid flow through packed columns. Chemical Engineering Progress 48 (2), 89–94.

Freund, H., Zeiser, T., Huber, F., Klemm, E., Brenner, G., Durst, F., Emig, J., 2003. Numerical simulations of single phase reacting flows in randomly packed fixed-bed reactors and experimental validation. Chemical Engineering Science 58 (3–6), 903–910.

Guardo, A., Coussirat, M., Larrayoz, M.A., Recasens, F., Egusquiza, E., 2005. Influence of the turbulence model in CFD modeling of wall-to-fluid heat transfer in packed beds. Chemical Engineering Science 60 (6), 1733–1742.

Guardo, A., Coussirat, M., Recasens, F., Larrayoz, M.A., Escaler, X., 2006. CFD study on particle-to-fluid heat transfer in fixed bed reactors: convective heat transfer at low and high pressure. Chemical Engineering Science 61 (13), 4341–4353.

Guardo, A., Coussirat, M., Recasens, F., Larrayoz, M.A., Escaler, X., 2007. CFD studies on particle-to-fluid mass and heat transfer in packed beds: free convection effects in supercritical fluids. Chemical Engineering Science 62 (18–20), 5503–5511.

Gunjal, P.R., Ranade, V.V., Chaudhari, R.V., 2005. Computational study of a single-phase flow in packed beds of spheres. A.I.Ch.E. Journal 51 (2), 365–378.

Larachi, F., Petre, C.F., Iliuta, I., Grandjean, B.P.A., 2003. Tailoring the pressure drop of structured packings through CFD simulations. Chemical Engineering and Processing 42 (7), 535–541.

Lee, J.J., Park, G.C., Kim, K.Y., Lee, W.J., 2007. Numerical treatment of pebble contact in the flow and heat transfer analysis of a pebble bed reactor core. Nuclear Engineering and Design 237 (22), 2183–2196.

Nakayama, A., Kuwahara, F., Kawamura, Y., Koyama, Y.H., 1995. Three-dimensional numerical simulation of flow through a microscopic porous structure. ASME/JSME Thermal Engineering Conference, 313–318.

Nield, D.A., Bejan, A., 2006. Convection in Porous Media, third ed. Springer, New York.

Nijemeisland, M., Dixon, A.G., 2001. Comparison of CFD simulations to experiment for convective heat transfer in a gas-solid fixed bed. Chemical Engineering Journal 82, 231–246.

Nijemeisland, M., Dixon, A.G., 2004. CFD study of fluid flow and wall heat transfer in a fixed bed of spheres. A.I.Ch.E. Journal 50, 906–921.

Petre, C.F., Larachi, F., Iliuta, I., Grandjean, B.P.A., 2003. Pressure drop through structured packings: breakdown into the contributing mechanisms by CFD modeling. Chemical Engineering Science 58 (1), 163–177.

Romkes, S.J.P., Dautzenberg, F.M., van den Bleek, C.M., Calis, H.P.A., 2003. CFD modelling and experimental validation of particle-to-fluid mass and heat

transfer in a packed bed at very low channel to particle diameter ratio. Chemical Engineering Journal 96 (1–3), 3–13.
Suekane, T., Yokouchi, Y., Hirai, S., 2003. Inertial flow structures in a simple-packed bed of spheres. A.I.Ch.E. Journal 49 (1), 10–17.
Susskind, H., Becker, W., 1967. Pressure drop in geometrically ordered packed beds of spheres. A.I.Ch.E. Journal 13 (6), 1155–1159.
Wakao, N., Kaguei, S., 1982. Heat and Mass Transfer in Packed Beds. McGraw-Hill, New York.
Yakhot, V., Orszag, S.A., 1986. Renormalization group analysis of turbulence: basic theory. Journal of Scientific Computing 1 (1), 3–11.